ELSEVIER

International Journal of Heat and Fluid Flow 20 (1999) 355–367

International Journal of
HEAT AND
FLUID FLOW

www.elsevier.com/locate/ijhff

Turbulent heat transfer measurements using liquid crystals ☆

Peter T. Ireland, Andrew J. Neely, David R.H. Gillespie *, Andrew J. Robertson

Department of Engineering Science, University of Oxford, Parks Road, Oxford, OX1 3PJ, UK

Received 18 November 1998; accepted 16 March 1999

Abstract

The transient method of measuring heat transfer coefficients that uses liquid crystals, since its beginnings in the early 1980s, has become one of the best ways of determining full surface distributions of heat transfer coefficient. The turbomachinery research group at Oxford has concentrated on the application of the method to numerous mechanical engineering thermal problems specific to the jet engine. The paper summarises some of the recent developments in the technique including the implementation of an elegant way of producing a change in the fluid temperature. Recent, high-density heat transfer coefficient measurements are discussed together with the advantages such resolution offers in terms of flow field interpretation. A means of integrating the measurements into finite element software for subsequent data analysis is presented. The paper should be of interest to engineers interested in using the most modern heat transfer measurement techniques in their research and development programmes.

Notation

c_p	specific heat at constant pressure for air, J/kg K
c	specific heat of perspex, J/kg K
d	hole diameter, m
h	heat transfer coefficient, W/m^2 K
I	current, A
k	thermal conductivity of perspex, W/m K
m	mass flow rate, kg/s
t	time, s
T	temperature, °C
V	voltage, V

Greek

η	mesh convective efficiency
ρ	density, kg/m^3
τ	time constant, s

Subscripts

g	gas
m	mesh wire temperature
O	starting
s	surface

1. Background

The transient liquid crystal method of measuring heat transfer to thermally insulating models of mechanical engineering components is one of the most effective ways of measuring complete distributions of local heat transfer coefficient. Its advantages include the provision of data over the complete surface in one experiment, its high accuracy, and the ease of model manufacture. Encapsulated cholesteric liquid crystals can be used as surface thermometers in a range of temperatures lying between −30°C and 150°C, crystals typically used in experiments display a full scale colour change over a range of either 1°C ('narrow band') or 20°C ('wide band'). In their optically active phase, intermolecular forces cause adjacent layers of molecules to align themselves at a slight angle to each other and this results in a helical arrangement of a particular pitch. This pitch decreases with increasing temperature. Light of wavelength of the same order as the pitch is selectively reflected from the model surface. The liquid crystals have a response time constant of approximately 3 ms (Ireland, 1987). The experimental accuracy depends on both the experimental conditions and the sophistication of the image processing applied to the liquid crystal colour play. In its most straightforward implementation, the uncertainty in heat transfer coefficient is about 6%, see Baughn et al., 1988; Byerley, 1988, though image processing that uses the full time content of the video data can improve this. When local heat transfer coefficients processed in an image are referenced to an accurately known heat transfer coefficient at some position in the video image, the accuracy in heat transfer coefficient ratio can be very high (approximately 2% uncertainty), see Wang et al. (1994). The latter were the first to use colour processing in transient heat transfer experiments and they demonstrated the advantages of using a liquid crystal material with a calibrated response over approximately 15°C. The point heat transfer coefficient referred to above is determined using a continuous record of surface temperature measured using a flat sensor such as a thin film gauge or a foil thermocouple. Such sensors are

* Corresponding author. Tel.: +44-1865 288 761; fax: +44-1865 288 756

☆ The work in this paper was presented at the Engineering Foundation Turbulent Heat Transfer Conference 2, Manchester, 1–4 June 1998.

0142-727X/99/$ – see front matter
PII: S0142-727X(99)00030-2

used by the authors in all heat transfer experiments as they a1so enable the liquid crystal material to be calibrated in situ.

As the basic technique is well established only a brief description is given here for the sake of completeness. In the heat transfer experiments, scale models of engine components are manufactured from a poor thermal conductor, a transparent plastic such as perspex (PMMA) allows excellent optical access. The liquid crystal coating (typically of thickness ~10 micron) is applied to the substrate using a small air brush and the optical response can be made insensitive to coating thickness. Only a limited number of surface point thermometers (usually thermocouples) are required for crystal calibration and the determination of the model initial temperature. This simplifies model construction and installation. The model is situated in a wind tunnel in which the flow temperature can be different to the model starting temperature. Flow is initiated, or the temperature of an established flow is changed, and the model temperature starts to change. The liquid crystal colour play at the surface is recorded using video equipment. These data are subsequently digitised frame by frame and the colour play history of each pixel yields the temperature history of the model surface, and hence the local heat transfer coefficient distribution.

The ease with which the surface coating can be prepared, even if the model surface has compound curvature, makes the method particularly suitable to the measurement of heat transfer coefficients on complex shaped surfaces. Examples of measurements from complicated shapes include Chyu et al. (1997) who used the method to measure the heat transfer coefficient to dimples used to promote heat transfer in internal cooling passages, Fig. 1. Wang et al. (1995) investigated the heat transfer coefficient distribution over an isolated pedestal (or pin fin) with fillet radii, Fig. 2. In both of the above cases, no other heat transfer method would have been capable of providing full distributions of local heat transfer coefficient. The technique still offers advantages for flat surfaces. Recent examples of external heat transfer coefficients include Robertson et al. (1997) and Robertson et al. (1998a). Fig. 3 shows the heat transfer coefficient map on a set of flat fins aligned parallel to the air flow. The benefits of interrupting the fins is apparent from Fig. 4.

2. Establishment of the thermal transient (Figs. 5–19)

2.1. Earlier strategies

Numerous strategies have been used to establish the temperature difference between the fluid and the model starting temperature to drive the heat transfer process. Early experimental arrangements included large electrical heaters that took time to stabilise at the required temperature, Clifford et al. (1983). The heat transfer measuring method is better conditioned if the fluid temperature undergoes a sudden change at the start of the test. For this reason, the heater time constant was overcome by using plumbing which allowed the flow to by-pass the test section whilst the electrical heaters obtained a steady temperature. Fast acting valves were then switched to start the heat transfer experiment, Fig. 5. Other approaches include rapidly inserting a model into the wind tunnel, Throckmorton and Stone (1974). The large-scale annular blow-down facility at Oxford uses a pair of shutters to isolate the instrumented section of the annulus from the substantial flow, Martinez-Botas et al. (1995), Fig. 6. The perspex vanes are preheated (or pre-cooled) in thermal isolation from the major flow before the test begins. The test flow is then established by rapidly withdrawing the shutters.

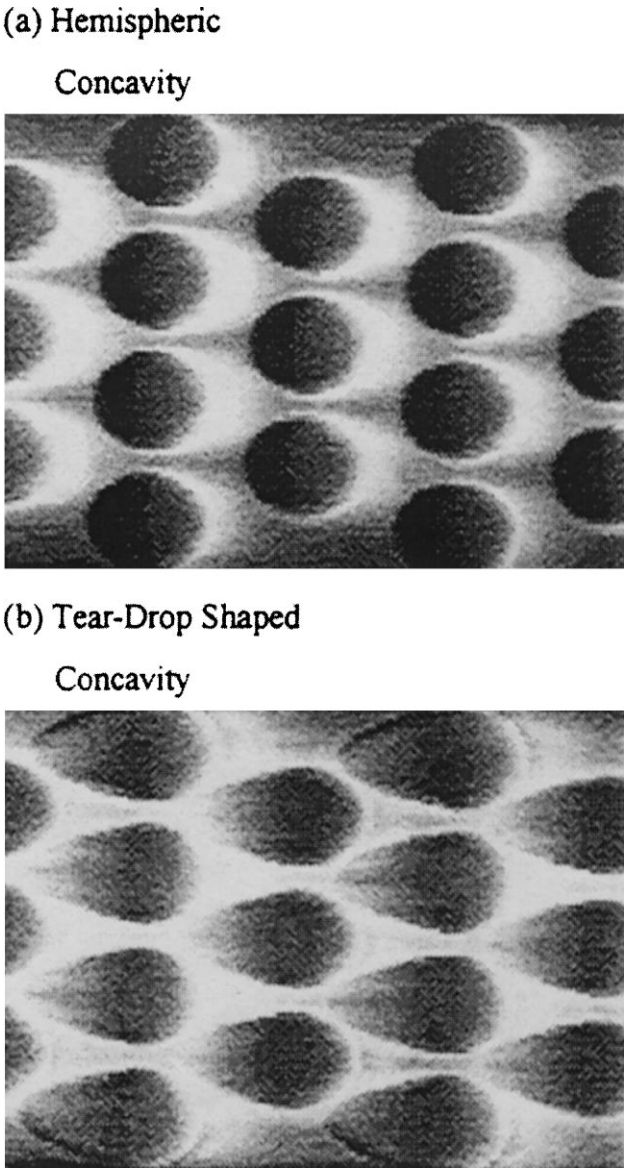

Fig. 1. Heat transfer coefficient distribution measured on a dimpled surface by Chyu et al. (1997).

2.2. Mesh heater concept

In many of the heat transfer tunnels at Oxford, the switched flow systems have been replaced by a fine electrical heater invented by Gillespie et al. (1995), Fig. 7. The heater spans the duct and changes the flow temperature over a very short distance in the flow direction. Facility construction is considerably simplified since the mechanical complexities of fast acting valves or model positioning activators are avoided. The surprising feature of the mesh heater is the high convective efficiency. The mesh convective efficiency, defined as

$$\eta = \frac{T_{\text{downstream}} - T_{\text{upstream}}}{T_{\text{mesh}} - T_{\text{upstream}}}$$

depends on the air speed, but in the case shown in Fig. 13 (at 5 m/s) η is approximately 0.55. This means that the wire overheat can be modest and problems associated with hot wires in the tunnel are avoided. The wires do not sag appreciably and

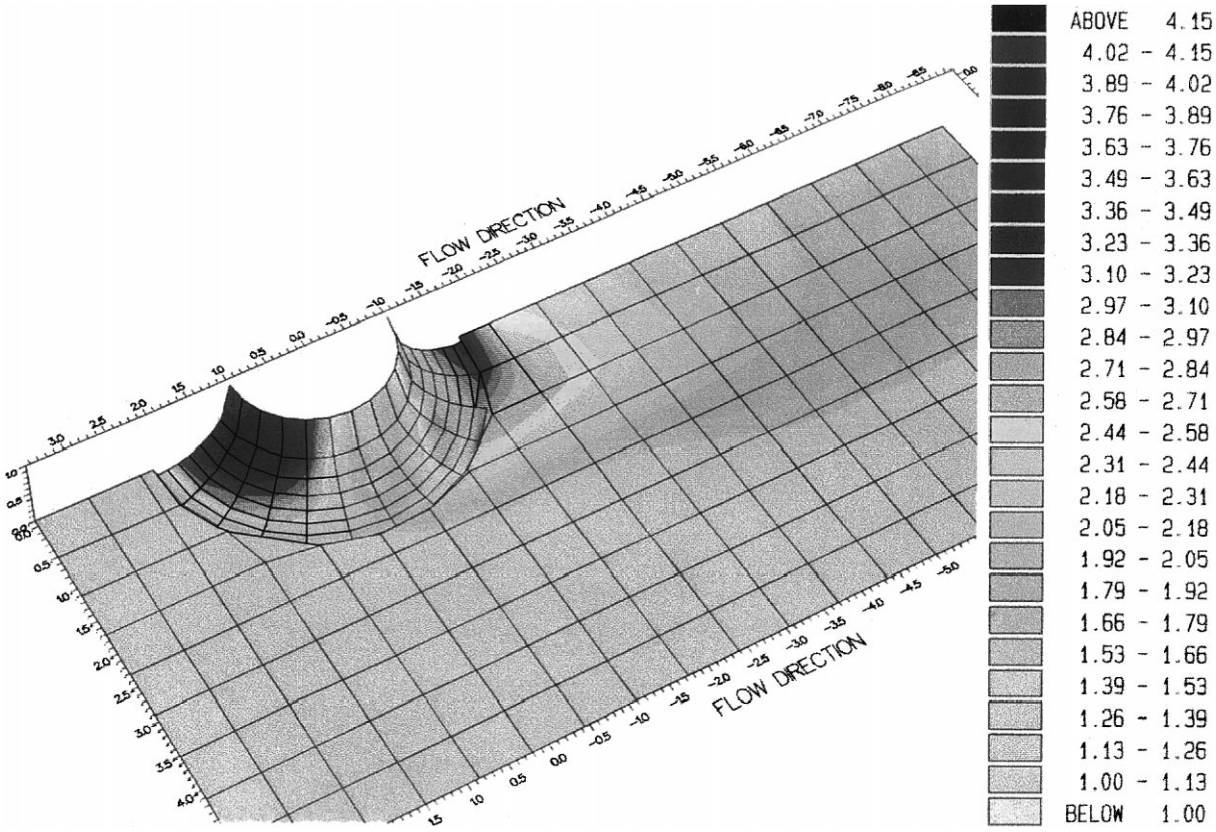

Fig. 2. Heat transfer coefficient measured over the surface of a pedestal with fillet radii, after Wang et al. (1995).

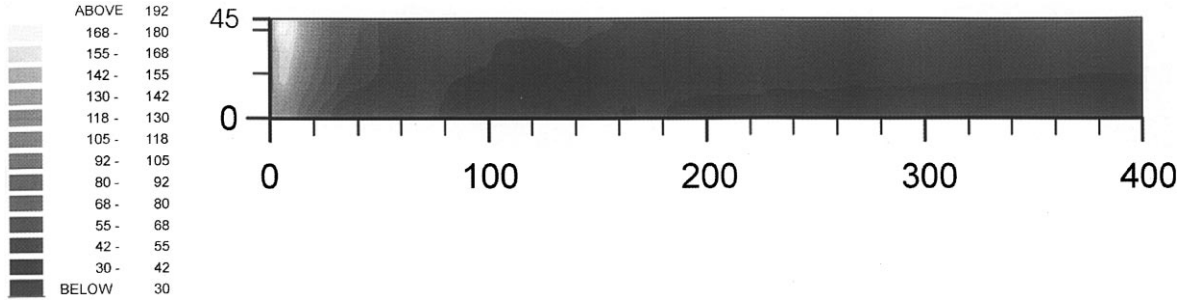

Fig. 3. Local heat transfer coefficient (Wm^{-2} K^{-1}), distribution on flat fins aligned with the flow, Robertson et al. (1997). The fin dimensions are marked in mm and flow is from left to right. ($s=12$ mm, $t=1.5$ mm, $w=45$ mm, $u=25.3$ m s^{-1}.)

radiated heat is minimal. Careful engineering of the mesh carrier ensures that the temperature of the wires is uniform so that a uniform flow temperature is achieved downstream. Fig. 13 is an image from an IR camera reflecting the mesh temperature. The indicated mesh temperature is uniform to within 1.3°C in this case where the flow temperature is being increased by 20°C. The non-uniformity in downstream temperature can be calculated as 3.5% of the temperature increase.

Gillespie et al. (1995) characterised the performance of the planar heaters and through a combination of theory and experiments, produced the chart of convective efficiency against air speed shown in Fig. 8. The meshes used employed 40 μm diameter wire which allows the mesh to run at a lower temperature than for thicker wires. The small diameter also ensures that any turbulence produced by the mesh is dissipated within a very short distance.

The most recent meshes have been used to heat moderately high pressure (~100 psi) air for further impingement research, Fig. 14. For a fixed mass flow rate, heating the air at higher upstream density is an effective means of reducing the mesh face velocity (for fixed area) and this allows the heater size to be reduced. The heater mesh in the figure is being used to rapidly switch the flow temperature in a programme of impingement cooling research. Of course, in situations where pressure loss needs to be minimised, the mesh area is kept large and the flow contracted downstream, Neely et al. (1998).

2.3. Mesh heater advantages

The mesh used has a through flow to projected area quotient of 0.38 and can, under correct lighting conditions, be translucent. Fig. 15 shows an arrangement used to measure

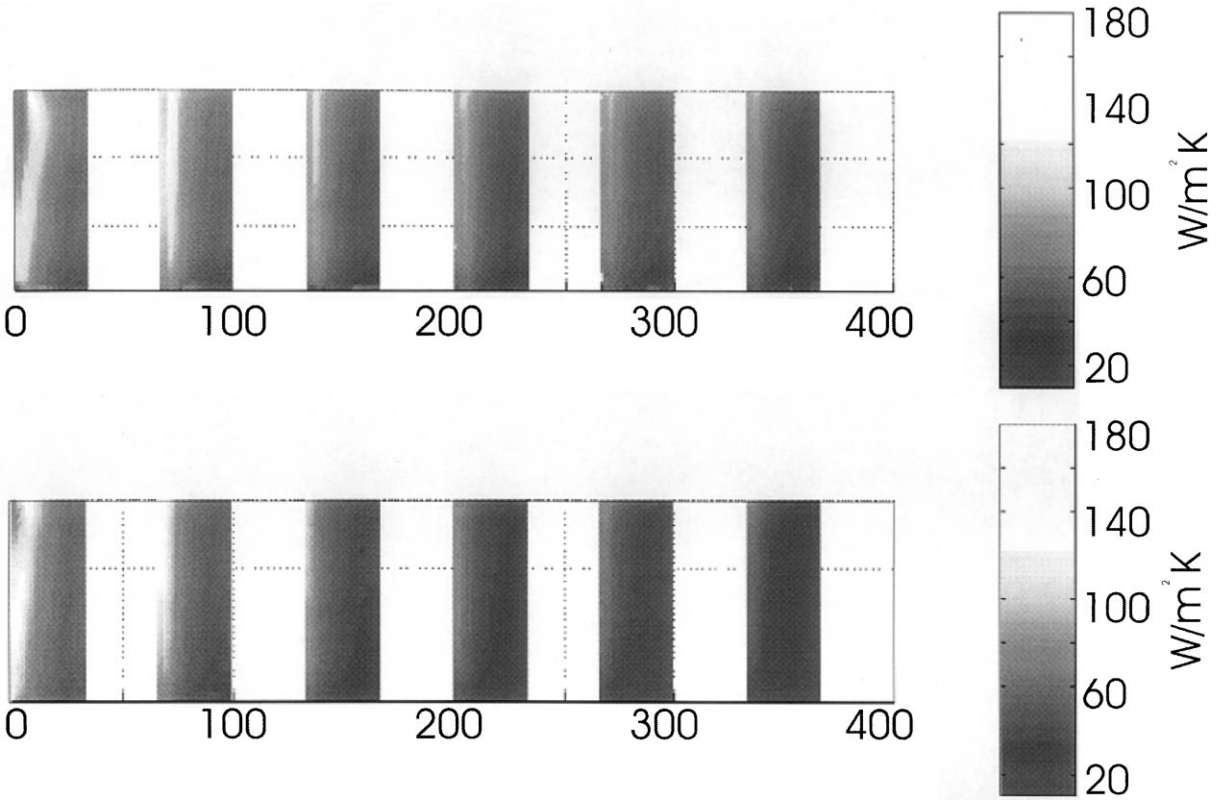

Fig. 4. Local heat transfer coefficient distribution on flat interrupted fins aligned with the flow, Robertson et al. (1997). The lower figure has half the spacing of the upper.

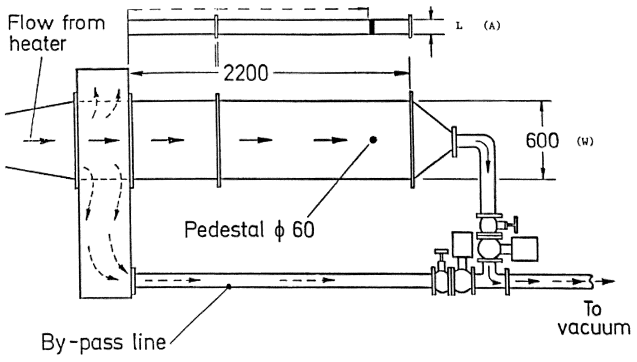

Fig. 5. Early arrangement used to produce the step change in fluid temperature, after Ireland (1987).

heat transfer coefficients to engine components where the flow is from a large nozzle through a polycarbonate perforated plate Neely et al. (1998). Fig. 16 shows an image of the liquid crystal coated perspex model taken from a miniature camera position inside the nozzle assembly. The camera looks through the mesh and the use of a wide camera aperture effectively removes the mesh from the image. The calculated heat transfer coefficient distribution is presented in Fig. 17. The same approach was previously used by Gillespie (1996) to measure the heat transfer coefficients on the upstream surface of an impingement plate, Fig. 18.

All of the electrical power supplied to the mesh heats the air so that an accurate measurement of the average temperature increase can readily be achieved by measuring the power supplied to the mesh.

$$T_{\text{downstream}} - T_{\text{upstream}} = \frac{IV}{mc_{\text{p}}}$$

This approach has proved very useful in low speed flow situations where the time response of the gas measuring thermocouple is prohibitively slow. Fig. 19 shows the level of agreement between the calculated and measured temperatures for recent blade cooling passage experiments, Tsang and Ireland (1998).

In some situations it may be desirable to generate a temperature profile using unheated, heated combinations of the mesh in series. This could allow profiles that have an artificially thick cool region near the wall to be produced. A summary of experimental rigs which have used a mesh heater to provide the thermal transient is given in Table 1.

2.4. Applications

The system has been used for research into turbine blade cooling systems, Gillespie et al. (1998); Gillespie (1996) and Wang et al. (1998), for investigating extended heat transfer surfaces for cooling engine components Neely et al. (1997); and for film cooling experiments Allen (1996). The largest mesh heater to date, Fig. 9, consumes more than 40 kW and is used to heat a high flow rate tunnel ($\sim$10 m^3/s) at speeds ranging from 5 to 30 m/s. This work has been reported in Neely et al. (1997) and led to the optimisation of extended surface shapes used to cool the outside of engine components (see Robertson et al., 1998a). In this case, the electrical power consumption was reduced by supplying current to only the central section of the duct. The powered section was then surrounded by two unpowered meshes and analysis was performed to ensure that the unheated flow did not encroach on

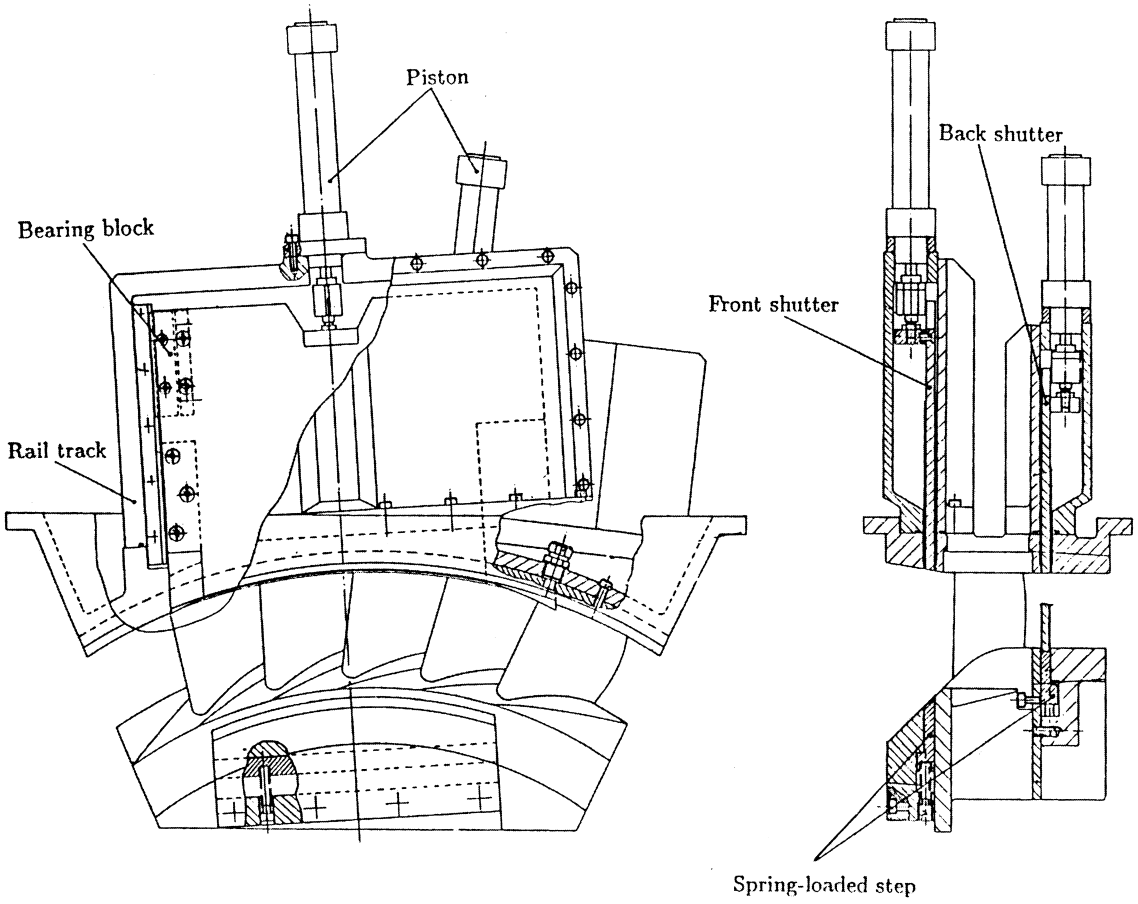

Fig. 6. Detail of the annular heat transfer facility used at Oxford to measure heat transfer coefficients to turbine nozzle guide vanes, from Martinez-Botas et al. (1995).

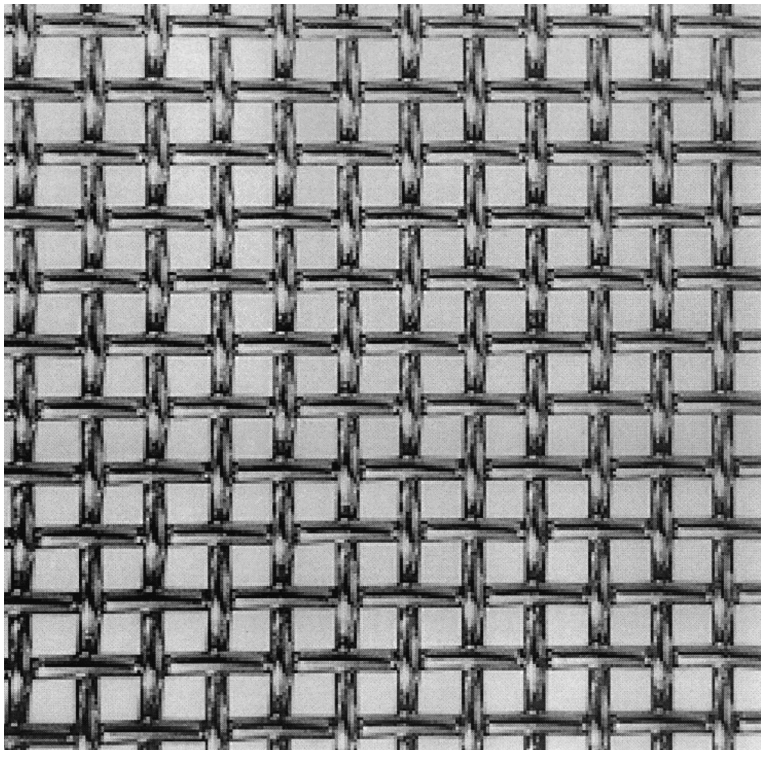

Fig. 7. Close up of heater mesh. Wire diameter is 40 μm.

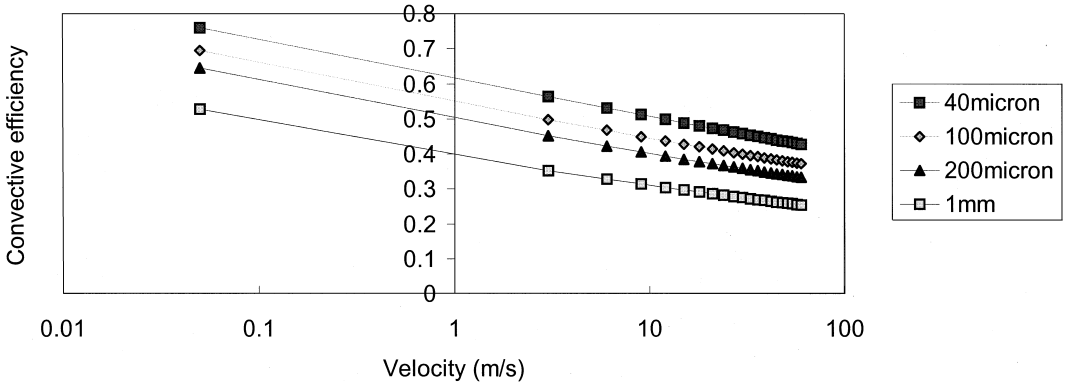

Fig. 8. Mesh convective efficiency as a function of flow speed. The meshes used employ 40 μm wire and the chart shows a prediction of the effect of changing wire diameter.

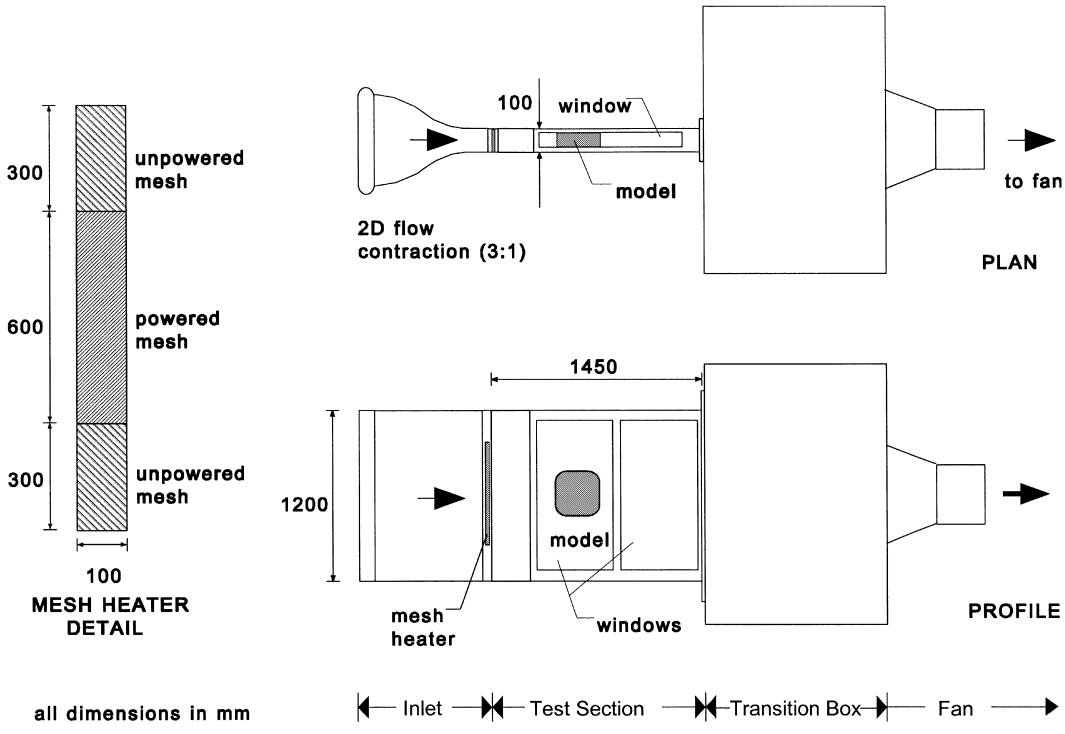

Fig. 9. Heat transfer tunnel used to investigate the thermal performance of extended surfaces.

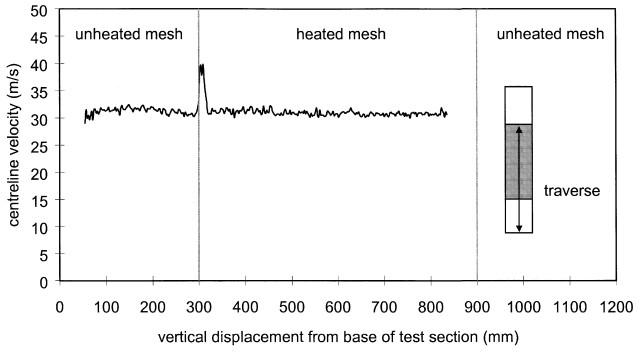

Fig. 10. Velocity profile measured 340 mm downstream of the heater mesh showing the edge of the heated and unheated sections.

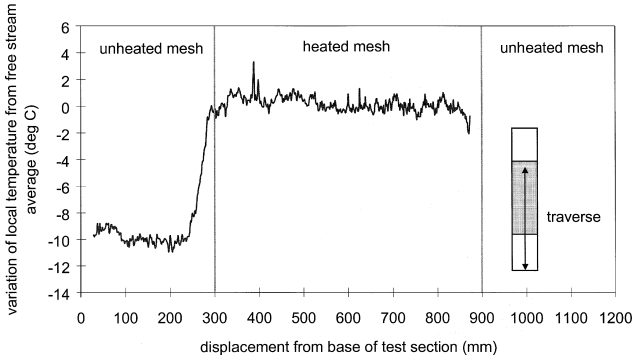

Fig. 11. Vertical temperature traverse measured 370 mm downstream of the heater mesh in extended surface research tunnel.

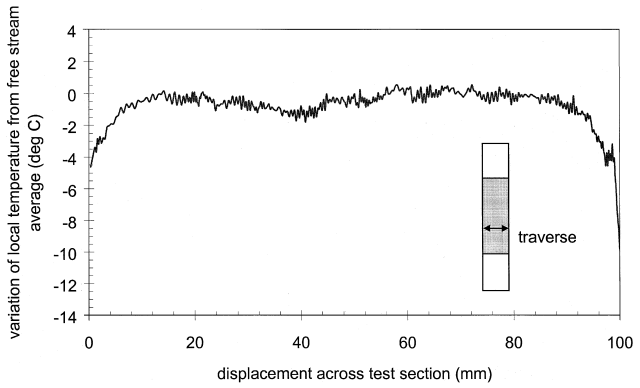

Fig. 12. Horizontal temperature traverse measured 370 mm downstream of the heater mesh in extended surface research tunnel (130 mm below the centreline).

the centrally positioned heat transfer model. A small (~1 mm) gap prevented current passing from the central to the surrounding meshes. Fig. 10 shows the velocity measured 340 mm downstream of the mesh and clearly shows the small jet caused by the gap between the unheated and the heated meshes. The affect on the flow temperature can be seen in Fig. 11 where the unheated and heated zones are clearly denoted. The small jet temperature will be between that of the heated and unheated zones and does not show up clearly in this figure.

Heat transfer measurements in impingement systems are difficult for a number of reasons. The local heat transfer coefficient changes by a large factor from a peak at the stagnation point beneath the jet to significantly lower values away from the jet in the channel between impingement and target plate. One difficulty specific to the transient method is the problem of quickly establishing the flow at a temperature different to the starting temperature. In a typical impingement array, the area ratio between the plenum feeding the jets and the total cross-sectional area of the jets means that the flow velocity in the plenum is very low (typically 0.1 m/s). This is the region in which flow switching needs to be performed and this leads to problems. Van Treuren et al. (1994) used a complicated by-pass system that passed heated air into the plenum for 30 min prior to the start of the transient experiment. The test section was prevented from pre-heating by bleeding room temperature air through the model into the plenum. Three electrically operated fast acting valves were synchronised to initiate the transient heat transfer experiment. The flow temperature switching in later impingement heat transfer experiments is now achieved using a planar heater mesh fitted across the plenum flow. The apparatus no-longer requires any fast acting valves since the experiments start when power is switched to the mesh. Prior to this stage, room temperature air is drawn through the heater mesh and model.

The velocity through the heater mesh in impingement experiments is typically low and a step change in the power supplied does not cause the flow temperature to change as a step. The normal surface temperature response of the perspex substrate under a step change in fluid temperature is given by the familiar equation

$$T_s = T_0 + (T_g - T_0)\exp\left(\frac{h^2 t}{\rho c k}\right)\mathrm{erfc}\left(\frac{h\sqrt{t}}{\sqrt{\rho c k}}\right)$$

When the heat transfer driving fluid temperature changes with a time constant, τ, the equation for the surface temperature rise becomes, Gillespie (1996),

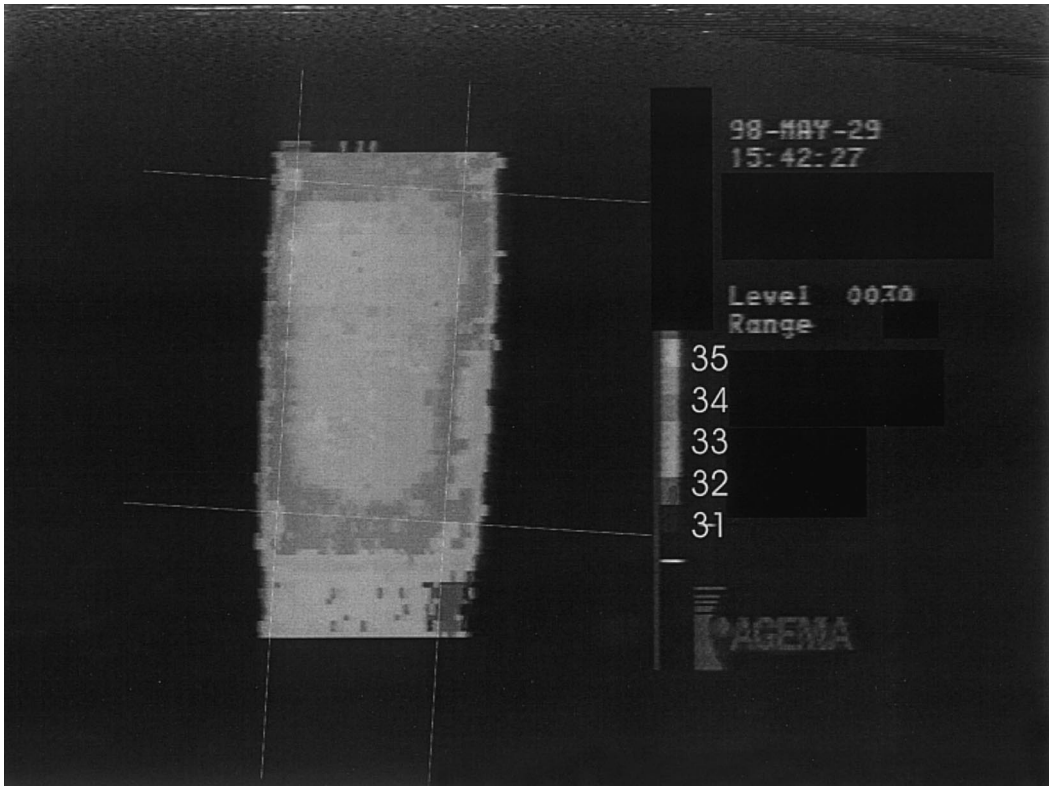

Fig. 13. IR image of the heater mesh fitted to the plenum of the rig used to make the heat transfer measurements to the impinging jets. The extent of the mesh is indicate by the white lines and the surrounding signals are reflections from the rig intake.

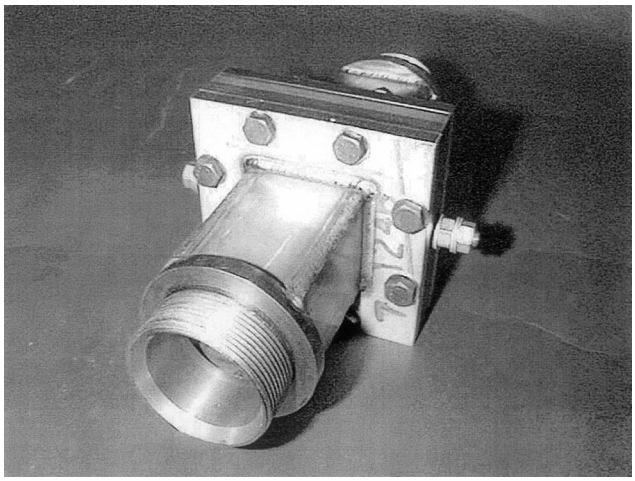

Fig. 14. Heater mesh arrangement used to heat high pressure air. Pipe i.d. is 50 mm.

$$\frac{T}{T_g} = 1 - \frac{\rho ck/h^2\tau}{(1+\rho ck/h^2\tau)}\ e^{h^2t/\rho ck}\mathrm{erfc}\left(\frac{h\sqrt{t}}{\sqrt{\rho ck}}\right) - e^{-t/\tau}\frac{1}{(1+\rho ck/h^2\tau)} \times\left(1+\frac{\sqrt{\rho ck}}{h\sqrt{\tau}}\left(\frac{1}{\pi}\sqrt{\frac{t}{\tau}}+\frac{2}{\pi}\sum_1^\infty\frac{1}{n}\ e^{-n^2/4}\sinh\ n\sqrt{\frac{t}{\tau}}\right)\right)$$

The above equation is then solved numerically for the local heat transfer coefficients from the time, t, the surface takes to reach the known liquid crystal temperature. In situations when the gas temperature change is neither a step change nor a first order lag, the fluid temperature should be measured and the measured signal used in a numerical procedure that sums the surface response to multiple delayed steps, Metzger and Larson (1986), or multiple delayed ramps, Saabas et al. (1987).

3. Application to impingement cooling research

Progress in the hardware used at Oxford has centred around a change in the frame grabbing strategy. The card that digitises the video recording is fitted to a Pentium PC and the data stored directly in computer RAM. The computer has 512 Mbytes of RAM and is capable of acquiring 500 full frames. In practice, not all pixel information is required to resolve accurately typical heat transfer coefficient results and this enables an even greater number of frames to be captured. In addition, not every frame is required for heat transfer processing. A typical heat transfer test lasts several seconds and the data is digitised over two or three sweeps. Each frame is captured at a particular time from the start of the heat transfer experiment. A time signal is captured in the frame and used to reference the intensity signal to the elapsed time.

4. Image processing – High resolution heat transfer coefficient data

Fig. 20 shows the heat transfer coefficient distribution on the target plate beneath an array of impinging jets. The work is notable for the high data resolution that shows the repeatability of the heat transfer coefficient signature between rows. The exit from the channel is from one side and spent flow from the early rows forms a cross-flow on the later jets. The research is reported further in Michaelis et al. (1998) and Son et al. (1998). To some extent the required heat transfer coefficient data resolution depends on the use to which the data will be put. For general engineering purposes, the resolution could be quite low: the component designer need only be confident that there are no significant excursions in local heat transfer coefficient levels which have not been processed that could cause problems in the application. The advantage of using a full surface coating is that such excursions in h distribution are immediately apparent, and be of great help in drawing conclusions about the flow field. It is also worth noting that the data resolution can be adjusted by altering the extent of the model viewed by the video camera. Hence,

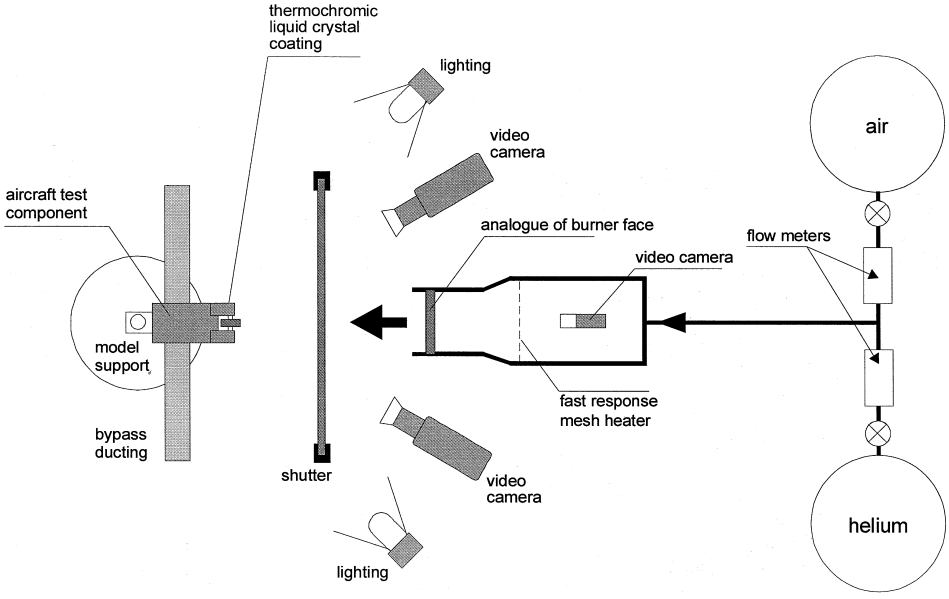

Fig. 15. Arrangement used to measure heat transfer coefficients to engine components. Flow is from large nozzle including a perforated plate.

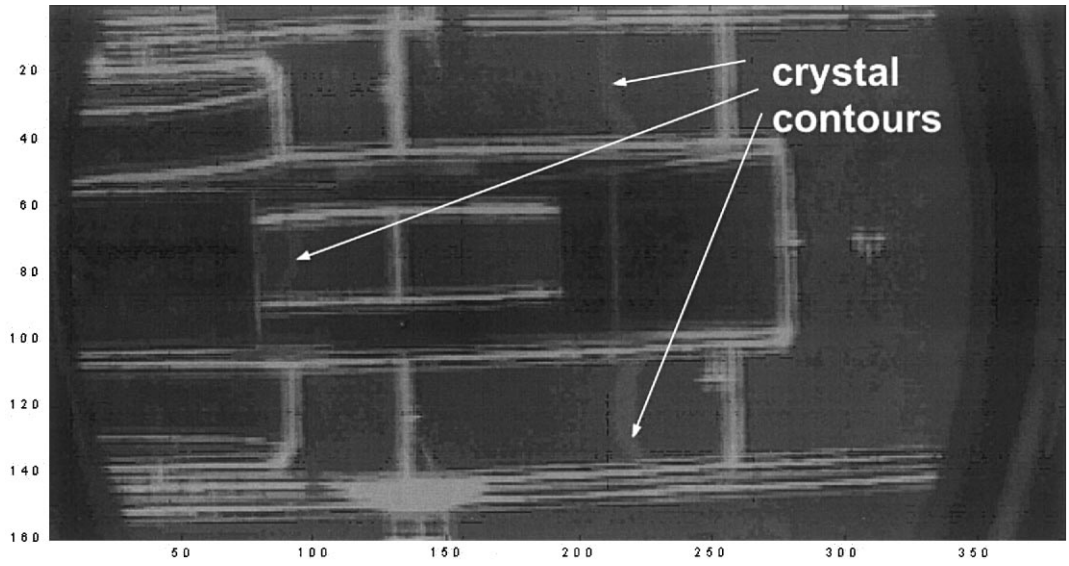

Fig. 16. Image of engine mount ring through the mesh and porous Perspex plate in fire test rig.

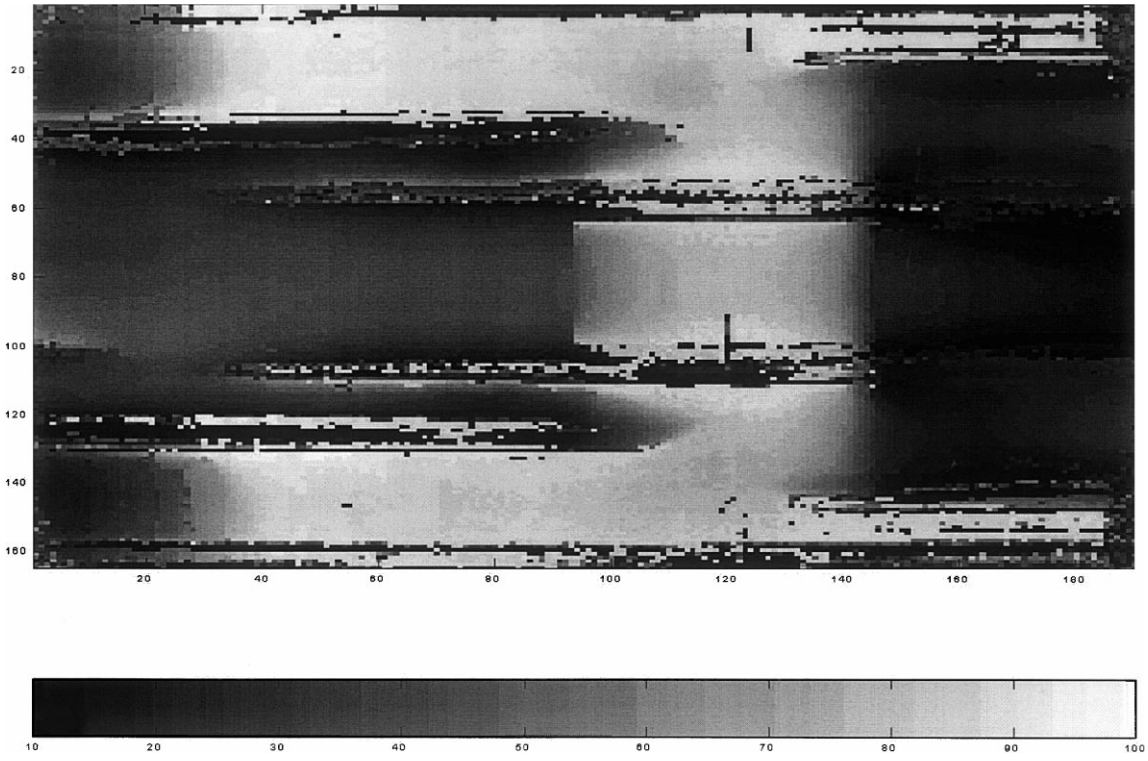

Fig. 17. Heat transfer coefficient distribution ($W/M^2/K$) deduced from video history of view through the mesh and porous perspex plate in the fire-test rig.

proper account can be taken of the high h zones following a preliminary test. The image processing strategy used in Fig. 20 was to apply a combination of three different narrow band liquid crystals that produce peaks in intensity at three calibrated temperatures at every pixel. Each image includes more than 5000 data points and the high data resolution can be seen to reveal interesting features about the flow field. The repeatability of the bump in heat transfer beneath each jet is very noticeable even though each jet is subjected to a differing amount of cross-flow. In this arrangement, three different hole sizes have been used. The first three rows of holes have the same diameter. The fourth and fifth rows have larger diameter holes. The last row has an even larger diameter. One feature that seems repeatable is the change in heat transfer coefficient slope present between $1.1d$ and $1.5d$ from the hole axis. This attenuation of the radial decay of the measured heat transfer coefficient is indicative of the position of boundary layer transition.

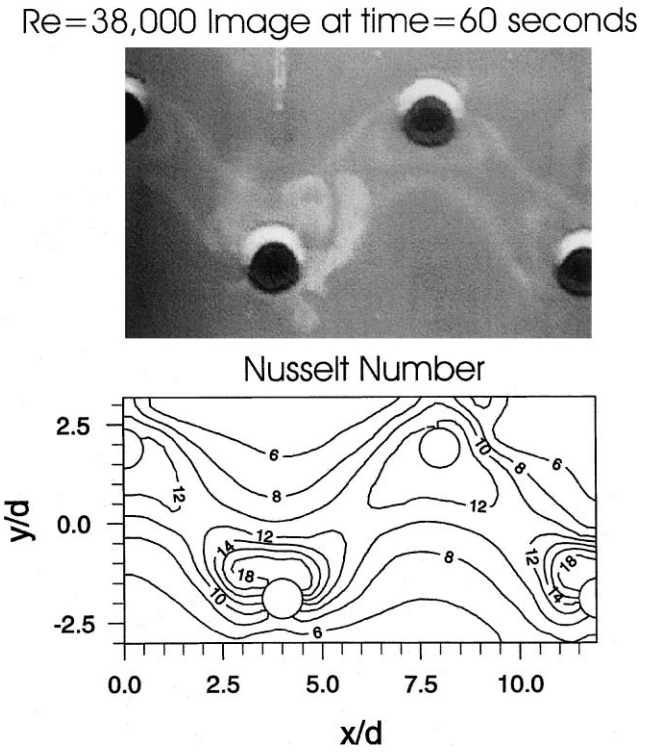

Fig. 18. Nusselt number contours on the front face of a plate used to produce impinging jets. The upper image is from a camera viewing through the heater mesh.

Earlier liquid crystal experiments at Oxford by Van Treuren tested an array with a bigger spacing between holes. His data, at a slightly lower resolution, exhibited the same shaped bumps beneath the jets. Fig. 21 shows present data normalised by the stagnation point heat transfer coefficient. The results from Van Treuren have also been included and, despite a hole spacing to diameter ratio more than twice the present value, there is remarkable similarity between the heat transfer coefficient variation. Van Treuren's measurements were made in a transient heat transfer facility in which the impingement plate was water cooled to maintain a constant temperature. The liquid crystal data were processed to obtain both the heat transfer coefficient and the adiabatic wall temperature. The latter was then expressed as a dimensionless temperature difference ratio. The present data were from a fully perspex rig in which the impingement plate was allowed to warm up during the experiment. The heat transfer driving temperature is then the temperature downstream of the heater mesh (the plenum temperature) as can be seen from the heat flux – temperature plot included as Fig. 22. The data here could be applied to systems in which the plate temperature is the same as the plenum temperature.

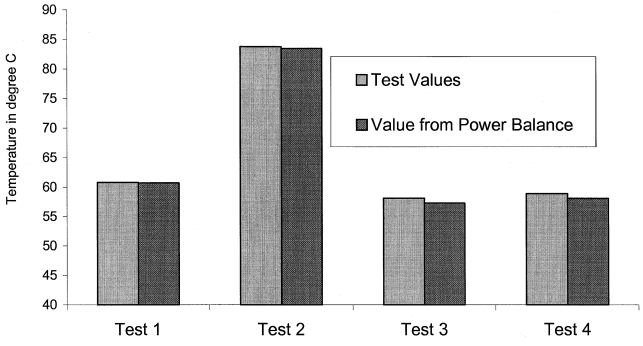

Fig. 19. Temperature increase (°C) calculated from power supplied versus measured fluid temperature increase for a typical blade cooling experiment. Note the false origin-temperature upstream of the mesh is approximately 20°C.

5. Data recovery from liquid crystal experiments

The subject of automatically recovering the liquid crystal colour change times from video recordings of experiments has been addressed by Robertson (1998b). The software links the co-ordinates of a numerically defined model into pixel co-or-

Table 1
Summary of applications of the heater mesh

Reference	Application	Flow speed range	Arrangement	Area (in mm)
Gillespie et al. (1998)	Wall cooling	<1 m/s	Small suck down tunnel. Used for impingement research.	300 × 450
Wang et al. (1998)	Ribs	10–18 m/s	Fitted to inlet of long, square section duct.	50 × 50
Allen (1996)	Film cooling	5–25 m/s	Small suck down tunnel (50 mm square section). Film cooling research.	55 × 55
Neely et al. (1997)	Extended surfaces (fins) on cylinders	5–25 m/s	Large suck down tunnel (10 kg/s).	100 × 600
Robertson et al. (1997)	Extended surfaces (fins) on flat plates	as Neely et al.	as Neely et al.	as Neely et al.
Fletcher (1997)	Interconnected hole cooling systems	~5 m/s	At entrance to long circular pipe. Latter used to produce developed conditions.	75 × 75
Fowler (1997)	Screen heater	<1 m/s	Intrinsically safe version for de-mist applications.	80 × 50
Son et al. (1998)	Impingement flow	<1 m/s	Used in impingement rig plenum.	280 × 310
Tsang and Ireland (1998)	Rib	10–18 m/s	Fitted to inlet of long, square section duct.	as Wang et al.
Mee et al. (1998)	Aerofoil leading edge	<1 m/s	Fitted inside cylinder to pre-heat flow to films.	60 × 60
Neely et al. (1998)	Fire certification (hot side)	<0.5 m/s	Helium/air flow. Used in analogue burner.	178 × 178
Neely et al. (1998)	Fire certification (cold side)	65–85 m/s	Fitted before contraction to reduce pressure loss. Flow velocity is test section velocity.	300 × 350

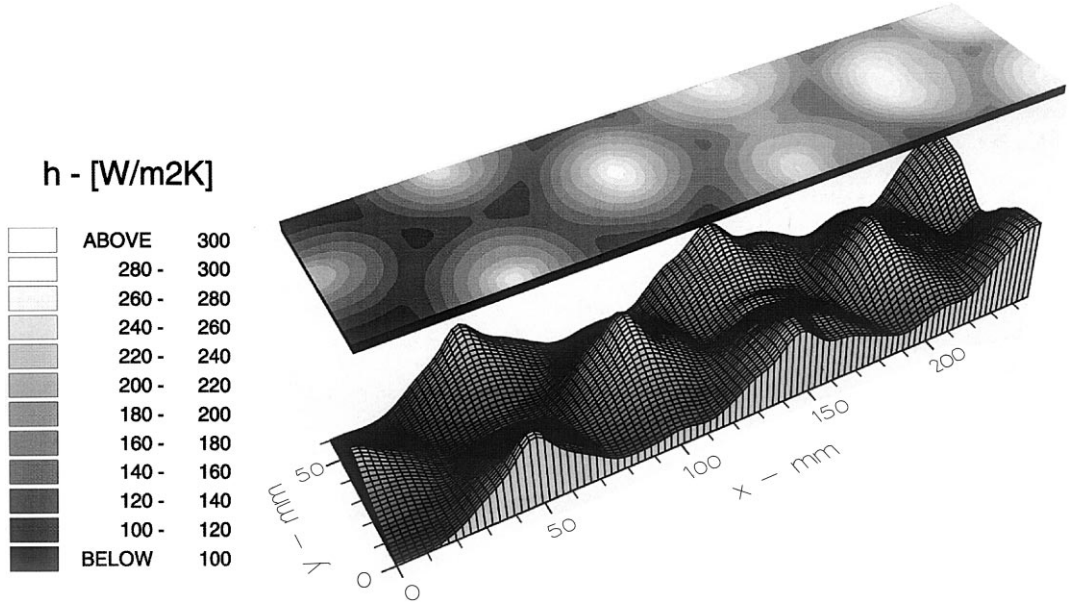

Fig. 20. Detailed heat transfer coefficients on the target plate beneath an engine representative array of impinging jets. The flow exits from one side of the channel in the direction of the arrow.

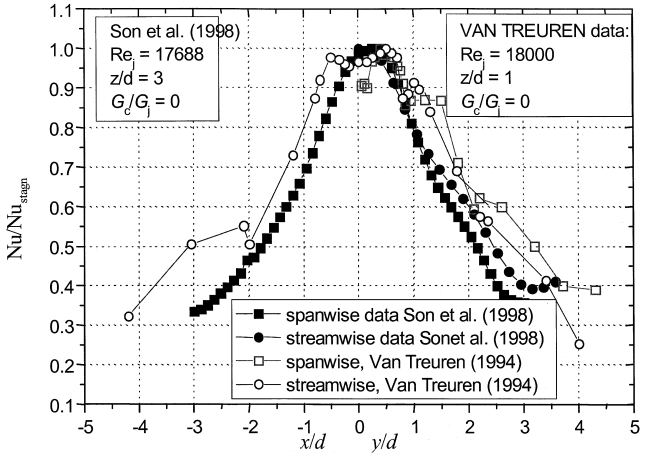

Fig. 21. Comparison of normalised heat transfer coefficient for impingement arrays with very different spacing.

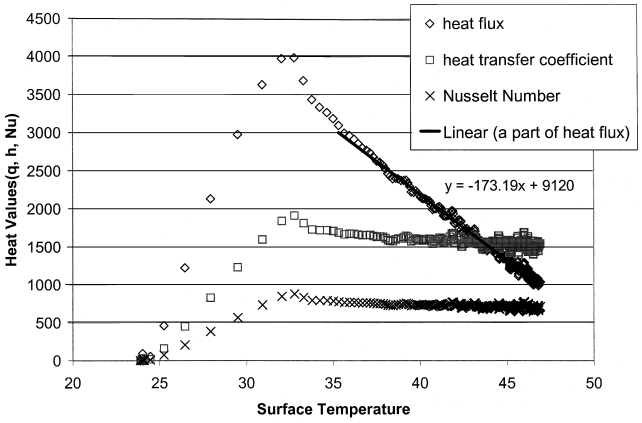

Fig. 22. Heat flux versus surface temperature.

dinates using an analytic model of the optical system. An example of the integration of a finite element software package with video images of a liquid crystal coated perspex model of an engine component is shown in Fig. 23. Software recognition of occluded surfaces allows video data to be mapped to the model geometry. When linked to the heat-transfer-solving program, the software can automatically extract the measured heat transfer coefficients in real co-ordinates. This has proved invaluable for finite element analyses of real engine components where the actual temperature is influenced by lateral conduction occurring in a metallic component, and a subsequent conduction analysis is required.

6. Conclusions

The paper summaries recent progress in what has become an established method of measuring distributions of local heat transfer coefficient. Since its introduction three years ago, the mesh heater has rapidly replaced other heaters as a very convenient (and hence low cost) way of producing the thermal transient. The paper describes the mesh and gives several recent applications of its use. The translucent nature of the mesh has allowed camera views through the heater and examples are given of the use of this advantage. The uniformity of the mesh has been discussed and a means of reducing the total electrical power by including unpowered sections presented. The mesh has been shown to be suitable for heating atmospheric and super-atmospheric flow. The mesh has been used to research the one of the most difficult cooling systems: that of impingement cooling. In this situation, the change in driving temperature is achieved easily and the need for complicated plumbing to pre-heat the plenum avoided. Progress in the image processing has increased the data point resolution. A very exciting computational method for determining the co-ordinates of points on 3-D model surfaces at which the crystal changes colour has been introduced.

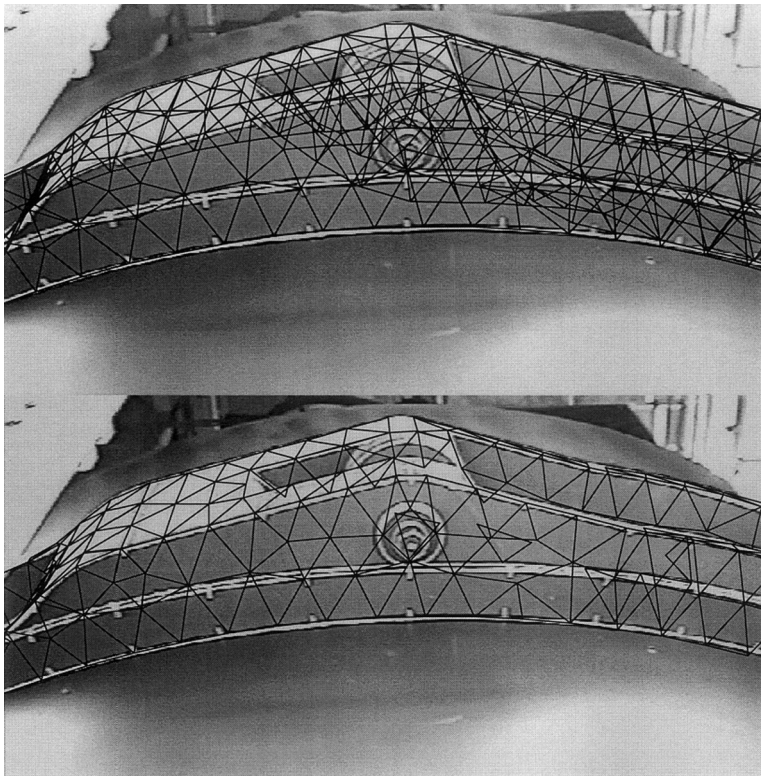

Fig. 23. An example of the integration of a finite element software package with video images of a perspex model of an engine component. The lower figure has hidden lines removed automatically.

Acknowledgements

Some of the research described here was supported by Rolls-Royce plc. and the Ministry of Defence (DERA Pyestock). The Rhodes foundation are also due thanks for supporting Andrew Robertson through his doctoral research.

References

Allen, C., 1996. A computational and experimental examination of film cooling. D. Phil thesis, University of Oxford.

Baughn, J.W., Ireland, P.T., Jones, T.V., 1988. A comparison of the transient and heated-coating methods for the measurement of local heat transfer coefficients. ASME paper, 88-GT-180 and later in the J. Turbomachinery, 1988.

Byerley, A.R., 1988, Heat transfer near the entrance to a film cooling hole in a gas turbine blade. D. Phil thesis, Department of Engineering Science, University of Oxford.

Chyu, M.K., Yu, Y., Ding, H., Downs, J.P., Soechting, F.O. 1997. Concavity enhanced heat transfer in an internal cooling passage. ASME paper 97-GT-437.

Clifford, R.J., Jones, T.V, Dunne, S.T. 1983. Techniques for obtaining detailed heat transfer coefficient measurements within gas turbine blade and vane cooling passages. ASME paper 83-GT-58.

Fletcher, D.A., 1997. Internal cooling of turbine blades, the matrix cooling method. D.Phil thesis, University of Oxford.

Fowler, J.D., 1997. Compact heater for de-misting applications. Final year project, Dept. Engineering Science., University of Oxford.

Gillespie, D.R.H., Wang, Z., Ireland, P.T. 1995. Heating Element. British Patent Application PCT/GB96/2017.

Gillespie, D.R.H., 1996. Intricate internal cooling systems for gas turbine blading. D.Phil thesis, University of Oxford.

Gillespie, D.R.H., Wang, Z., Z, Ireland, P.T., Kohler, S.T., 1998. Full surface local heat transfer measurements in a model of an integrally cast impingement cooling geometry. J. Turbomachinery 120, 92–99.

Ireland, P.T., 1987. Internal cooling of turbine blades, D.Phil thesis, University of Oxford.

Martinez-Botas, R.F., Lock, G.D., Jones, T.V., 1995. Heat transfer measurements in an annular cascade of transonic gas turbine blades using the transient liquid crystal technique. J. Turbomachinery 117, 425–431.

Mee, D.J., Ireland, P.T., Bather, S. 1998. Measurement of the temperature field downstream of simulated leading-edge film-cooling holes, Experiments in Fluids (to be published).

Metzger, D.E., Larson, D.E., 1986. Use of melting point surface coatings for local convection heat transfer measurements in rectangular channel flows with 90 degree turns. J. Heat Transfer 108, 48–54.

Michaelis, M., Robertson, A.J., Ireland, P.T. 1998. Detailed heat transfer coefficient measurements in an engine representative impingement cooling system. OUEL report.

Neely, A.J., Ireland, P.T., Harper, L.R. 1997. Extended surface convective cooling of engine components using the transient liquid crystal technique. J. Power and Energy, 211, A, 273–287.

Neely, A.J., Ireland, P.T., Mullender, A. 1998. Validation of novel low-temperature fire event modelling technique. Royal Aeronautical Society conference: Verification of design methods by test and analysis, 23–24th November, 1998.

Robertson, A.J., Neely, A.J., Ireland, P.T. 1997. Local heat transfer coefficients on flat continuous, interrupted and corrugated external fins. ASME paper 97-GT-380 presented at I.G.T.I. conference, Orlando, 1997.

Robertson, A.J., Neely, A.J., Ireland, P.T., Harper, L.R. 1998a. Local coefficients of heat transfer on optimised finned cylinders, Pro-

ceedings of the 36th Aerospace Sciences meeting, Reno, January 12–15, paper AIAA 98-0875.

Robertson, A.J., 1998b. Extended surface heat transfer performance. D.Phil thesis, University of Oxford.

Saabas, H.J., Arora, S.C., Abdel Messeh. 1987. Application of the transient test technique to measure local heat transfer coefficients associated with augmented airfoil cooling passages. ASME paper 87-GT-212.

Son, C.M., Michaelis, M., Robertson, A.J., Ireland, P.T., 1998. Detailed heat transfer coefficient measurements in an engine representative impingement cooling system using liquid crystals. presented at the Int. Mech. Eng. Congress and Expo. Anaheim CA.

Throckmorton, D.A., Stone, D.R., 1974. Model wall and recovery temperature effects on experimental heat transfer data analysis. AIAA 12, 169–170.

Tsang, C.L., Ireland, P.T. 1998. Temperature variation in a long passage during a transient heat transfer experiment. OUEL report.

Van Treuren, K.V., Wang, Z., Ireland, P.T., Jones, T.V. 1994. Local heat transfer coefficient and adiabatic wall temperature measurements beneath arrays of staggered and inline impinging jets. ASME paper 94-GT-181.

Wang, Z., Ireland, P.T., Jones, T.V., Davenport, R., 1994. A colour image processing system for transient liquid crystal heat transfer experiments. ASME J. Turbomachinery 118, 421–427.

Wang, Z., Ireland, P.T., Jones, T.V., 1995. Detailed heat transfer measurements and thermal analysis at engine conditions of a pedestal with fillet radii. J. Turbomachinery 117, 290–297.

Wang, Z., Ireland, P.T., Kohler, S.T., Chew, J., 1998. Heat transfer measurements to a gas turbine cooling passage with inclined ribs. J. Turbomachinery 120, 63–69.